

Ultra compact dwarf galaxy formation by tidal stripping of nucleated dwarf galaxies

J. Pfeffer^{1*} and H. Baumgardt¹

¹*School of Mathematics and Physics, The University of Queensland, Brisbane, QLD 4072, Australia*

ABSTRACT

Ultra Compact Dwarf Galaxies (UCDs) and dwarf galaxy nuclei have many common properties, such as internal velocity dispersions and colour-magnitude trends, suggesting tidally stripped dwarf galaxies as a possible UCD origin. However, UCDs typically have sizes more than twice as large as nuclei at the same luminosity. We use a GPU-enabled version of the particle-mesh code SUPERBOX to study the possibility of turning nucleated dwarf galaxies into UCDs by tidally stripping them in a Virgo-like galaxy cluster. We find that motion in spherical potentials, where close passages happen many times, leads to the formation of compact ($r_h \lesssim 20$ pc) star clusters/UCDs. In contrast, orbital motion where close passages happen only once or twice leads to the formation of extended objects which are large enough to account for the full range of observed UCD sizes. For such motion, we find that dwarf galaxies need close pericentre passages with distances less than 10 kpc to undergo strong enough stripping so that UCD formation is possible. As tidal stripping produces objects with similar properties to UCDs, and our estimates suggest dwarf galaxies have been destroyed in sufficient numbers to explain the observed number of UCDs in M87, we consider tidal stripping to be a likely origin of UCDs. However, comparison with cosmological simulations is needed to determine if the number and spatial distribution of UCDs formed by tidal stripping matches the observations of UCDs in galaxy clusters.

Key words: methods: *N*-body simulations – galaxies: dwarf – galaxies: formation – galaxies: interactions – galaxies: star clusters

1 INTRODUCTION

Ultra compact dwarf galaxies (UCDs) are a class of stellar systems that was discovered in the Fornax galaxy cluster more than a decade ago (Hilker et al. 1999a; Drinkwater et al. 2000). Since then, UCDs have been discovered in other galaxy clusters (Mieske et al. 2004; Hasegan et al. 2005; Jones et al. 2006; Mieske et al. 2007; Misgeld et al. 2011; Madrid 2011; Penny et al. 2012), galaxy groups (Evstigneeva et al. 2007b; Da Rocha et al. 2011), as well as isolated spiral galaxies (Hau et al. 2009). UCDs are typically defined to have half-light radii $7 \lesssim r_h/\text{pc} \lesssim 100$ and masses $M \gtrsim 2 \times 10^6 M_\odot$ (Mieske et al. 2008), making them an intermediate object between globular clusters (GCs) and dwarf galaxies.

The formation mechanism of UCDs is currently unknown, although a number of scenarios have been proposed. The simplest explanation is that they are the high-mass end of the GC mass function observed around galaxies with rich GC systems (Mieske, Hilker & Infante 2002; Mieske, Hilker & Misgeld 2012). Since UCDs have

larger sizes than typical GCs, they may form from the merger of many GCs (Kroupa 1998; Fellhauer & Kroupa 2002; Brüns et al. 2011; Brüns & Kroupa 2012). Alternatively, they could be dwarf galaxies stripped by tidal interactions such that only their central nuclei remain, referred to as the tidal stripping or “threshing” scenario (Bassino, Muzzio & Rabolli 1994; Bekki, Couch & Drinkwater 2001; Bekki et al. 2003; Drinkwater et al. 2003). There is also evidence suggesting UCDs are formed by a combination of mechanisms rather than a single one (Mieske et al. 2006; Brodie et al. 2011; Chilingarian et al. 2011; Norris & Kannappan 2011).

Tidally stripped dwarf galaxies, in particular nucleated dwarf elliptical galaxies (dE,Ns), have been proposed as UCD progenitors for a number of reasons: UCDs and dwarf elliptical nuclei have similar internal velocity dispersions (Drinkwater et al. 2003) and colour-magnitude trends (Côté et al. 2006; Evstigneeva et al. 2008; Brodie et al. 2011). UCDs lie above the metallicity-luminosity trend for early-type galaxies and have a similar metallicity to dwarf galaxies (Chilingarian et al. 2011; Francis et al. 2012). Such a situation would be expected if UCDs are tidally stripped dwarf galaxies since the luminosity would decrease while

* E-mail: j.pfeffer@uq.edu.au

the metallicity remains high. In addition, some UCDs are surrounded by stellar haloes which might be the remnants of the stripped dwarf galaxies (Drinkwater et al. 2003; Hasegan et al. 2005; Chilingarian & Mamon 2008; Evstigneeva et al. 2008; Chiboucas et al. 2011). Finally, irregular objects with asymmetric extensions have been found which may be dwarf galaxy nuclei undergoing tidal stripping (Richtler et al. 2005; Brodie et al. 2011).

Simulations of UCD formation in the tidal stripping scenario were first performed by Bekki et al. (2001, 2003), who showed that nucleated dwarf galaxies orbiting in a galaxy cluster on highly eccentric orbits are almost completely tidally stripped, with only the nucleus surviving. In this case the size and luminosity of the stripped galaxy are such that it would be classified as a UCD. More recently, Goerdt et al. (2008) sought to understand UCD formation by tidal stripping within the context of the cold dark matter (CDM) model, and found the cosmological prediction matches the observed spatial distribution of UCDs.

Despite this, a number of potential problems with the tidal stripping scenario still remain unanswered. Brodie et al. (2011) have recently found a population of extended, low mass UCDs ($r_h \sim 40$ pc, $M_V \sim -9$) in the Virgo galaxy cluster which do not follow the size-magnitude relation observed for the most massive UCDs (Mieske et al. 2006; Evstigneeva et al. 2008). Such objects may form from merged star cluster complexes (Brüns et al. 2011; Brüns & Kroupa 2012), however it is unclear whether they can be formed in either the giant GC or tidal stripping scenario.

UCDs are typically ~ 2 times larger than dE nuclei at the same luminosity (Evstigneeva et al. 2008). This suggests that if nuclei are the UCD progenitors the nuclei must undergo expansion, or some other process, during tidal stripping. The situation is even more pronounced for nuclei and UCDs with $M_V > -11$: at this luminosity the typical half-light radius of nuclei is ~ 4 pc, while UCDs extend up to ~ 40 pc (Brodie et al. 2011).

All tidal stripping simulations to date have been performed in static, spherical galaxy potentials with a constant pericentre and apocentre (Bekki et al. 2001, 2003; Goerdt et al. 2008), thus it is uncertain what effect an evolving or triaxial potential has on the number and properties of the UCDs that form in this scenario. In addition, these studies did not investigate if tidal stripping of dwarf galaxies affects the nucleus size, thus the origin of the size difference between UCDs and dE nuclei is still uncertain.

In this paper we perform high resolution N -body simulations of a nucleated dwarf galaxy being stripped via tidal interactions to test whether the extended, low mass UCDs can be formed in the tidal stripping scenario. We simulate orbits with fixed pericentres and apocentres, as well as orbits that mimic ‘box orbits’ in an evolving or triaxial potential, to study the effect of the dwarf galaxy’s orbit on the final size of the stripped dwarf galaxy.

2 THE SIMULATIONS

2.1 Simulation code

All simulations were performed with a graphics processing unit (GPU) enabled version of the particle-mesh code su-

PERBOX (Fellhauer et al. 2000) on NVIDIA GPUs. SUPERBOX uses a leap-frog scheme to integrate the motion of particles and has high-resolution subgrids which stay focused on the simulated objects. In SUPERBOX the density grids are derived using a nearest-grid-point (NGP) scheme. Potentials are calculated from the density grids using a Fast Fourier Transformation, which are performed in parallel across the subgrids using multiple GPUs. The forces are calculated using a NGP scheme based on the second derivatives of the potential. We have increased the subgrid number from 2 to 4 in order to accurately resolve the innermost regions of our dE,N models and reduce edge effects for particles crossing between subgrids. For the simulations we use 64^3 grid points for all subgrids with an innermost subgrid size of 0.013 kpc for model 1 and 0.025 kpc for models 2 and 3, and subsequent grid sizes of 0.05, 0.5, 4 and 40 kpc for all models. Time steps are chosen such that no particle moves more than a grid cell length of the smallest subgrid per time step. We use time steps of 0.004 Myr, 0.008 Myr and 0.006 Myr for dE,N models 1, 2 and 3, respectively.

2.2 Cluster mass profile

In order to have a realistic mass profile for the galaxy cluster, we model M87, the central galaxy of the Virgo cluster, based on the observations of Kormendy et al. (2009) and Murphy, Gebhardt & Adams (2011) using Sérsic and logarithmic profiles for the stellar and dark matter components, respectively. The Sérsic (1963, 1968) surface brightness profile is given by

$$I(R) = I_0 e^{-b(R/R_e)^{1/n}} \quad (1)$$

where I_0 , R_e and n are the central intensity, the effective half-light radius and the Sérsic index describing the curvature of the profile, respectively. The constant b is chosen such that R_e contains half the projected light and we use the relation between b and n found by Prugniel & Simien (1997). For the simulations the Sérsic surface brightness profile is converted into a potential using the method of Terzić & Graham (2005). We adopt for the stellar component a Sérsic index $n = 11.84$, an effective radius $R_e = 16.22$ kpc and a central intensity $I_0 = 2.732 \times 10^{17} L_\odot \text{ kpc}^{-2}$, consistent with Kormendy et al. (2009), and a mass-to-light ratio $\Upsilon = 9.1 (M/L)_\odot$ consistent with Murphy et al. (2011).

The logarithmic potential of the dark matter halo is given by

$$\phi(r) = \frac{v_c^2}{2} \ln(r_c^2 + r^2) \quad (2)$$

where r_c is the core radius and v_c is the asymptotic circular velocity. We adopt a scale radius $r_c = 36$ kpc and a circular velocity of $v_c = 800 \text{ km s}^{-1}$ consistent with Murphy et al. (2011).

For the cluster potential we choose a static, spherical potential similar to what has been chosen by other authors (Bekki et al. 2001, 2003; Goerdt et al. 2008). In order to add a time varying or triaxial component to the cluster potential it would be necessary to add more parameters to the simulations. In addition, in order to take into account substructure in the cluster which could perturb the orbits of the dwarf galaxy, it would be necessary to simulate a full galaxy cluster. Therefore, to reduce unnecessary complexity in the

Table 1. Parameters of the initial dwarf galaxy (columns 2-5) and the resulting UCD (columns 6-8) for all simulations. dE,N model 1 has a nucleus half-light radius $r_h = 4$ pc and magnitude $M_V = -10$ (nucleus mass $M_{\text{nuc}} = 2.56 \times 10^6 M_\odot$). dE,N model 2 has a nucleus half-light radius $r_h = 10$ pc and magnitude $M_V = -10$ (nucleus mass $M_{\text{nuc}} = 2.56 \times 10^6 M_\odot$). dE,N model 3 has a nucleus half-light radius $r_h = 10$ pc and magnitude $M_V = -12$ (nucleus mass $M_{\text{nuc}} = 1.62 \times 10^7 M_\odot$). Masses are converted to magnitudes assuming a mass-to-light ratio $\Upsilon = 3 (M/L_V)_\odot$.

Simulation no.	Orbit type	dE,N Model	Apocentre (kpc)	Pericentre (kpc)	Close pericentre passages	Final r_h (pc)	Final M_V (mag)	Formation time (Gyr)	Simulation time (Gyr)
1	Elliptic	1	50	2	5	3.9	-9.77	0.9	2.2
2	Elliptic	1	50	5	7	5.5	-10.10	1.3	2.2
3	Elliptic	1	50	10	12	6.6	-10.12	2.3	4.2
4	Elliptic	1	50	20	27	8.6	-10.14	5.7	7.5
5	Elliptic	1	100	2	5	4.2	-9.71	1.6	3.9
6	Elliptic	1	100	5	9	6.1	-10.07	2.9	3.9
7	Elliptic	1	100	10	15	7.6	-10.14	5.0	5.9
8	Elliptic	2	50	2	6	5.6	-9.02	1.1	2.2
9	Elliptic	2	50	5	7	9.5	-9.86	1.3	2.2
10	Elliptic	2	50	10	11	11.7	-10.02	2.1	4.2
11	Elliptic	2	50	20	25	18.7	-10.32	5.2	7.5
12	Elliptic	2	100	2	6	5.9	-9.07	1.9	3.9
13	Elliptic	2	100	5	9	10.3	-9.90	2.9	3.9
14	Elliptic	2	100	10	17	15.2	-10.19	5.6	5.9
15	Elliptic	3	50	2	5	7.0	-11.43	0.9	2.2
16	Elliptic	3	50	5	6	12.0	-12.01	1.1	2.2
17	Elliptic	3	50	10	9	15.5	-12.13	1.7	4.2
18	Elliptic	3	50	20	15	24.3	-12.30	3.1	7.5
19	Elliptic	3	100	2	5	7.7	-11.31	1.6	3.9
20	Elliptic	3	100	5	6	13.9	-12.04	1.9	3.9
21	Elliptic	3	100	10	11	19.3	-12.16	3.6	5.9
22	Box	1	50	2	1	28.3	-10.84	2.0	2.2
23	Box	1	50	2	2	7.7	-10.30	1.3	2.2
24	Box	1	50	5	2	49.8	-11.10	1.1	2.2
25	Box	1	50	5	3	14.6	-10.61	1.1	2.2
26	Box	1	100	2	1	94.1	-11.36	1.9	3.9
27	Box	1	100	2	2	9.7	-10.33	2.2	3.9
28	Box	1	100	5	2	179.0	-12.22	1.6	3.9
29	Box	1	100	5	3	58.1	-11.11	2.6	3.9
30	Box	2	50	2	1	46.3	-10.86	1.2	2.2
31	Box	2	50	2	2	13.4	-10.09	1.4	2.2
32	Box	2	50	5	2	59.6	-11.10	0.9	2.2
33	Box	2	50	5	3	25.1	-10.58	1.1	2.2
34	Box	2	100	2	1	98.2	-11.37	1.9	3.9
35	Box	2	100	2	2	17.1	-10.21	2.2	3.9
36	Box	2	100	5	2	168.0	-12.13	1.7	3.9
37	Box	2	100	5	3	65.8	-11.12	2.0	3.9
38	Box	3	50	2	1	28.7	-12.50	1.2	2.2
39	Box	3	50	2	2	15.0	-12.15	0.5	2.2
40	Box	3	50	5	2	32.1	-12.59	1.3	2.2
41	Box	3	50	5	3	20.5	-12.38	0.7	2.2
42	Box	3	100	2	1	65.8	-12.80	1.9	3.9
43	Box	3	100	2	2	18.7	-12.21	1.0	3.9
44	Box	3	100	5	2	118.0	-13.08	2.2	3.9
45	Box	3	100	5	3	37.7	-12.60	1.6	3.9

simulations, we mimic these possible situations by changing the orbit of the dE,N during the simulations. We discuss the dwarf galaxy orbits in more detail in Section 2.4.

2.3 Nucleated dwarf ellipticals

We construct three models for dE,Ns according to values observed for dEs in the Virgo cluster. The model number for each simulation is shown in column 3 of Table 1. The nucleus

is modelled using a King (1962) profile with a concentration parameter $c = 1.5$, with the value of c chosen since it is a typical value for GCs (Trager, King & Djorgovski 1995) which are similar in size to dE nuclei. An absolute V -band magnitude $M_V = -10$ is used for the nucleus of dE,N models 1 and 2, and $M_V = -12$ is used for model 3. For dE,N model 1 we use a nucleus half-light radius $r_h = 4$ pc (the average radius at this luminosity, see Fig. 2), while for models 2 and 3 we use $r_h = 10$ pc. The magnitude $M_V = -10$ is chosen

to be comparable to the low luminosity UCDs observed by Brodie et al. (2011), even though the least luminous UCDs observed by Brodie et al. have $M_V = -9$. We chose $M_V = -12$ to be comparable to a typical massive UCD. Note that the most massive UCDs have $M_V = -13$.

The main stellar component of the dwarf galaxy, referred to hereafter as the ‘envelope,’ is modelled using a Sérsic profile. For dE,N models 1 and 2 we use a Sérsic index $n = 1.5$ and an effective radius $R_e = 850$ pc, which are the average values observed by Grant, Kuipers & Philipps (2005) and Geha, Guhathakurta & van der Marel (2003) for dEs in the Virgo cluster, respectively, while for model 3 we use a Sérsic index $n = 1.5$ and an effective radius $R_e = 2000$ pc. The central intensity is chosen such that the nucleus-to-envelope luminosity ratio is 0.3%, the mean value for dEs in Virgo (Côté et al. 2006), giving an absolute V -band magnitude $M_V = -16.3$ for dE,N models 1 and 2, and $M_V = -18.3$ for dE,N model 3.

A mass-to-light ratio $\Upsilon = 3 (M/L_V)_\odot$ is set for both the nucleus and envelope, which is consistent with the average values observed by Chilingarian (2009). In order to reduce the number of particles needed, we do not include a dark matter halo for our dE,N models. We expect that including a cored dark matter profile in the models would not significantly affect our results for UCD sizes and masses since we are only interested in the centre of the model where the fraction of dark matter to stellar matter is lowest. This may not be the case if a cuspy dark matter profile was used since dwarf galaxies with cuspy dark matter profiles are more resilient to tidal stripping (Bekki et al. 2003; Peñarrubia et al. 2010). However, observations suggest dE galaxies do not have a significant amount of dark matter within one effective radius (Geha, Guhathakurta & van der Marel 2002), more consistent with a cored profile, justifying our neglect of a dark matter halo.

Although the simulated UCD sizes and masses would be unaffected by a dark matter halo, it is likely the inclusion of one would change the UCD formation time due to the dark matter shielding the stellar component from disruption (e.g. in Fig. 5 the envelope shields the nucleus during tidal stripping). Since a dark matter halo would be much more extended than the stellar component, we expect one to two close passages would be necessary to disrupt the halo and therefore add ~ 0.5 Gyr to the formation time. However, as a dwarf galaxy sized halo disrupts at a radius of a few hundred kpc in a galaxy cluster (Goerdts et al. 2008), it is possible that the halo is stripped before the dwarf galaxy reaches the centre of the cluster.

We create an N -body representation for the dwarf galaxies using the following method adapted from Hilker et al. (2007):

(i) Deprojection of the 2-dimensional surface density profile by means of the Abel integral equation (see equation 1B-57b of Binney & Tremaine 1987) into a 3-dimensional density profile.

(ii) Calculation of the cumulative mass function $M(< r)$ and the potential energy $\phi(r)$ from the 3-dimensional density profile. From these the energy distribution function $f(E)$ is then calculated with the help of equation 4-140a from Binney & Tremaine (1987), assuming isotropic orbits for the stars.

(iii) Creation of an N -body representation of the dE using the deprojected density profile and the distribution function.

The modelling is based on the assumptions of spherical symmetry and an underlying isotropic velocity distribution. For all dE,N models 10^7 particles with equal masses were distributed, corresponding to particle masses of $85.7 M_\odot$ with $2.56 \times 10^6 M_\odot$ contained in the nucleus for dE,N models 1 and 2, and particle masses of $541 M_\odot$ with $1.62 \times 10^7 M_\odot$ contained in the nucleus for model 3.

To test the stability of the models they were evolved in isolation for 2 Gyr. For model 2 the Lagrange radii are conserved to better than 4 per cent. For model 1 the half-light radius of the nucleus increases by 13 per cent due to numerical relaxation, however outside the central 30 pc the maximum radial change is less than 4 per cent. For model 3 the half-light radius of the nucleus increases by 12 per cent due to numerical relaxation while outside the central 45 pc the maximum radial change is less than 4 per cent.

2.4 Dwarf galaxy orbits

We test for nucleus expansion in the tidal stripping scenario with two types of orbits. First we assume that dE galaxies orbit the central galaxy on elliptic orbits with fixed apocentre and pericentre distances. For all dE,N models we test orbits with apocentres of 50 and 100 kpc and pericentres of 2, 5, 10 and 20 kpc. Such highly eccentric orbits are predicted by Λ CDM simulations for sub-haloes orbiting larger haloes (Ghigna et al. 1998).

Since elliptical galaxies are expected to reside in triaxial potentials and form through galaxy mergers, galaxy cluster potentials will be neither static nor spherical. The orbits of dwarf galaxies in such clusters may be chaotic with strongly varying pericentres distances during successive passages, either due to the triaxial potential or encounters with other galaxies during the orbit. Thus in addition to the elliptic orbit, we consider the case where only a few encounters between the dE and central galaxy will happen with very small pericentre distances, and at all other times the dE is far from the central galaxy so that tidal effects are not important. We mimic such a scenario by simulating 1-3 pericentre passages and then placing the object on a circular orbit at apocentre to allow enough time for unbound particles to escape. This is referred to hereafter as the ‘box’ orbit. For all dE,N models we test box orbits with apocentres of 50 and 100 kpc and pericentres of 2 and 5 kpc. Note we do not require that the orbits are circular (which is highly unlikely in Λ CDM), but only that the pericentre increases to $\gtrsim 10$ -20 kpc.

These two orbits represent the most extreme cases in the tidal stripping scenario, i.e. galaxies may have either many pericentre passages at small radii, or they have many passages at large radii and very few at small radii. It is probable that real UCDs will be on orbits somewhere in between these extremes.

The full list of simulations performed is shown in Table 1. The UCD formation time is defined as the time when the change in half-mass radius and mass within the tidal radius (calculated according to King 1962) of the resulting object falls below 10% between successive passages, while the final half-light radius and mass of the object is calculated at the end of the simulation (column 10 in Table 1). Since the

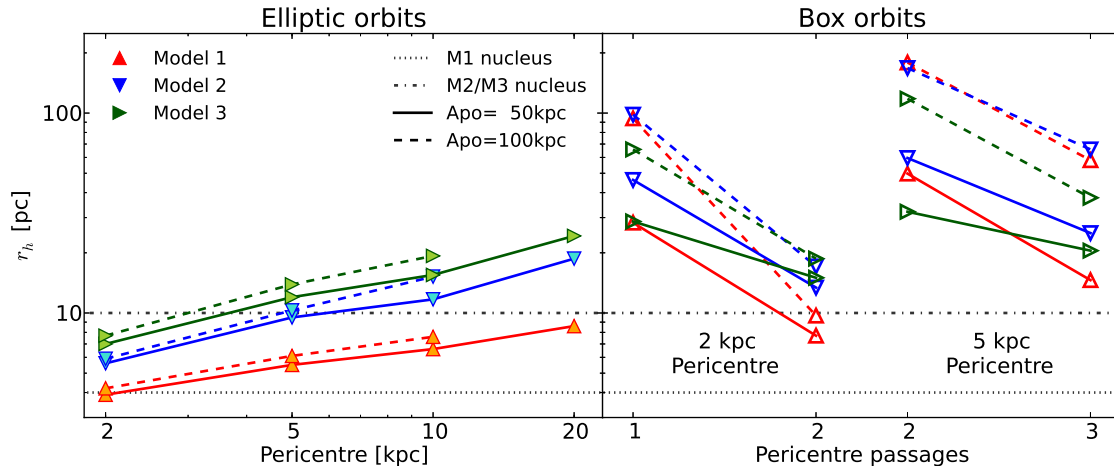


Figure 1. Comparison of the final half-light radii for all simulated UCDs in dependence of orbital type, dE,N model, and apocentre distance. The left panel shows the effect of pericentre distance for models on elliptic orbits, while the right panel shows the effect of pericentre distance and number of close pericentre passages for models on box orbits. Symbols are as in the legend, where triangle-up (red), triangle-down (blue) and triangle-right (green) denote dE,N model 1 (nucleus $r_h = 4$ pc, $M_V = -10$ mag), model 2 (nucleus $r_h = 10$ pc, $M_V = -12$ mag) and model 3 (nucleus $r_h = 10$ pc, $M_V = -12$ mag), respectively, and orbits with a 50 (100) kpc apocentre are represented by a solid (dashed) line. The dotted and dash-dot lines show the initial half-light radius of the nucleus for dE,N models 1 and 2/3, respectively.

change in the model is small at the end of the simulation (see Fig. 5) we can be confident that a longer simulation time will not significantly change our results. For the elliptic orbits the number of pericentre passages is the number before formation occurs and not the total number during the simulation.

3 RESULTS

3.1 Evolution of galaxy size

Fig. 1 shows a comparison of the final half-light radii for the simulated UCDs. Except for models on an elliptic orbit with a 2 kpc pericentre, all simulated UCDs have sizes larger than the initial model nucleus. All simulations, except for models on a box orbit with a 100 kpc apocentre and two pericentre passages at 5 kpc (simulations 26, 34 and 42), form objects with half-light radii less than 100 pc. For both elliptic and box orbits the half-light radius increases with pericentre distance since models with a small pericentre distance suffer more tidal stripping than those with a large pericentre distance. For a given pericentre distance, 100 kpc apocentres tend to produce larger half-light radii than 50 kpc apocentres because particles require more energy to escape the dwarf galaxy at a large galactocentric radius than at a small radius. Models on box orbits produce both larger half-light radii and a larger range of half-light radii than those on elliptic orbits ($10 \lesssim r_h/\text{pc} \lesssim 170$ for box orbits compared to $4 \lesssim r_h/\text{pc} \lesssim 25$ for elliptic orbits) due to box orbits having fewer close pericentre passages and therefore suffering less tidal stripping. In the box orbit scenario, an increase in the number of close pericentre passages results in a decrease in half-light radius due to the inner region of the model becoming more susceptible to tidal effects once the outer region has been removed.

Comparison of V -band magnitude and half-light radius

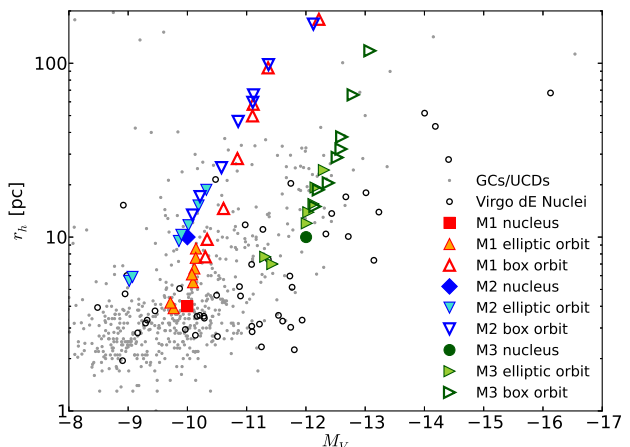


Figure 2. Final V -band magnitude and half-light radius for the simulated UCDs compared with GCs and UCDs from the nearby universe (Brodie et al. 2011, grey points), and Virgo dwarf elliptical nuclei (Côté et al. 2006, open black circles). The nuclei are converted to V -band photometry from g and z bands using the relation derived for M87 globular clusters by Peng et al. (2006). Symbols and colours are as in the legend, where M1, M2 and M3 are dE,N models 1, 2, and 3 runs, respectively, and the original model nuclei sizes are represented by a red square (M1), blue diamond (M2), and green circle (M3). The simulations are converted to a luminosity assuming a mass-to-light ratio $\Upsilon = 3$ (M/L_V) $_{\odot}$.

between the simulated UCDs and observed GCs, UCDs and dE nuclei is shown in Fig. 2. Note that the final UCD in the simulations is a combination of the remaining particles from both the nucleus and the envelope and therefore can be more massive than the initial nucleus. For dE nuclei with $M_V > -11$ the median half-light radius is 3.5 pc, and thus our model with a nucleus $r_h = 4$ pc (model 1) is more comparable to present day nuclei than the model with $r_h = 10$

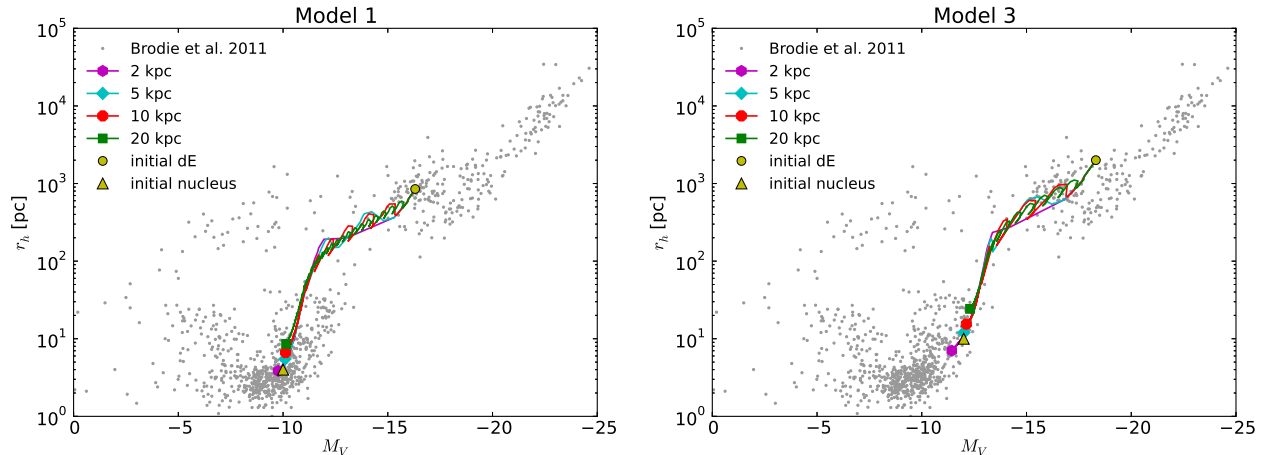


Figure 3. Morphology evolution of simulations on elliptic orbits with a 50 kpc apocentre for dE,N model 1 (left panel) and dE,N model 3 (right panel) compared to GCs, UCDs, dEs, dwarf spheroidals, compact ellipticals, and giant ellipticals from the nearby universe (Brodie et al. 2011, grey points). The V -band magnitude and half-light radius evolution of the models are shown as solid lines with a marker showing final UCD at the end of the simulation. The marker type and line colour for each simulation are as in the legend. The yellow circle and triangle mark the initial position of the dwarf galaxy and nucleus of the model, respectively.

pc (model 2). For dE nuclei with $M_V < -11$ the median half-light radius is 7.5 pc and thus comparable to the model with a nucleus $M_V = -12$ and $r_h = 10$ pc (model 3). In the elliptic orbit scenario the models have a maximum final half-light radius approximately less than two times the original nucleus size, and therefore can only match observed UCDs if dE nuclei have initial half-light radii $r_h \gtrsim 10$ pc. In principle the extended UCDs could be formed on elliptic orbits with pericentres larger than 20 kpc, however as formation time scales exponentially with pericentre distance, while UCD half-light radius scales as a power law with exponent ~ 0.5 with pericentre distance, the formation time required becomes much larger than a Hubble time for a dE,N with a nucleus size of $r_h \sim 4$ pc. In contrast, box orbits can produce half-light radii up to 40 times initial size of the model nucleus, and can produce the full range of observed UCD half-light radii with a nucleus half-light radius of either 4 or 10 pc. For model 3 the UCD sequence closely matches the most extended and massive UCDs ($-14 < M_V < -12.5$ and $60 < r_h/\text{pc} < 100$).

The morphological evolution from dE to UCD for models 1 and 3 on elliptic orbits is shown in Fig. 3. Model 2 simulations take a similar path in $r_h - M_V$ space as model 1 due to the models having an identical enclosed mass profile for the dE envelope. All simulations for a given dE,N model take a similar path in $r_h - M_V$ space, first towards lower mass and then towards lower radius, with only the end point along the sequence differing depending upon the orbital parameters. The figure shows that some objects classified as dwarf galaxies (i.e. objects with $r_h > 100$ pc) could have undergone some tidal stripping or are still being tidally stripped.

Figures 2 and 3 also show that our simulations predict the existence of objects with half-light radii between 50 and 200 pc and luminosities smaller than $M_V \sim -12$, while the catalogue from Brodie et al. (2011) lacks such objects. It is unclear whether this is a real effect or due to selection effects or selection bias, but note the catalogue compiled by

Brüns & Kroupa (2012) contains unconfirmed candidates in this region. If the extended, low mass UCDs form by tidal stripping, one would expect to see transition objects in the size gap. The absence or small number of objects in this region might imply different situations for UCD formation by tidal stripping: either the formation time is very short, or the tidal stripping occurred long ago, i.e. when the cluster formed. Our results show that UCDs on box orbits, which are necessary to form the extended UCDs, have typical formation times of 1-2 Gyr (see Table 1), in agreement with the first scenario. However, since most UCDs are ~ 10 -11 Gyr old (Evstigneeva et al. 2007a; Francis et al. 2012), while most dE nuclei are a few Gyr old (Paudel et al. 2011), this implies that most UCDs formed before the young dE nuclei were formed, otherwise one could expect to find more young UCDs. But note that dE nuclei with young ages might not be young at all, they might have formed long ago but had ongoing star formation or new star formation events at recent times. Therefore either of these points, or a combination of the two, may explain the lack of transition objects between dwarf galaxies and UCDs.

Fig. 4 shows a comparison of final half-mass radius and half the object mass for the simulations with the initial cumulative mass profile of the models and the final cumulative mass profile for box orbits with one pericentre passage at 2 kpc and a 50 kpc apocentre/circular orbit. If the origin of the size difference between UCDs and dE nuclei is due to expansion of the nucleus during tidal stripping the cumulative mass profiles of the final UCDs should differ from that of the initial nucleus of the model. Fig. 4 shows that the final UCD profiles differ little from nucleus of the initial models, and the mass and half-mass radius of the simulated UCDs trace the initial model nucleus, with the exception of the most massive UCDs for each model which have a significant stellar halo. This indicates expansion plays little role in the final UCD sizes. Although the model 1 elliptic orbit simulations show some deviation from the mass profile with increasing radius, this is most likely caused by numerical re-

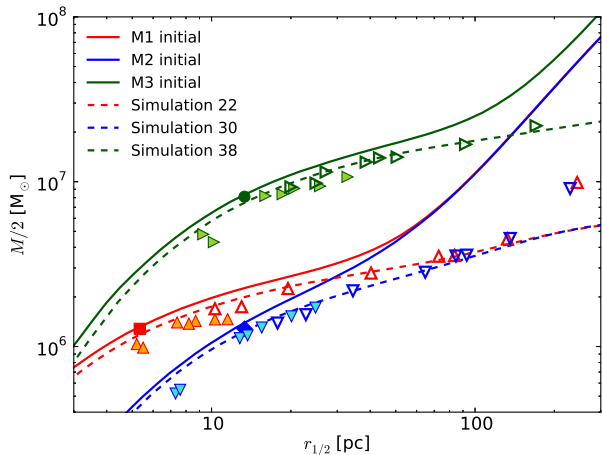


Figure 4. Final 3D half-mass radius ($r_{1/2}$) and half the object mass for all simulated UCDs compared with the initial cumulative mass profiles for the models (solid lines) and final cumulative mass profiles for simulations 22, 30 and 38 (box orbits with one pericentre passage at 2 kpc and a 50 kpc apocentre/circular orbit for models 1, 2 and 3 respectively, dashed lines). Colours and symbols are as in Figure 2.

laxation and not a real effect. Based on this result we expect that UCDs outside our sequence can be formed by models with different luminosities for the nucleus. Given the range of luminosities for dE nuclei in Fig. 2, the whole range of UCD sizes and luminosities could be produced by dE,N on box orbits.

3.2 UCD surface brightness profiles

As an example, Fig. 5 shows the surface brightness evolution for dE,N model 1 on an elliptic orbit with a 2 kpc pericentre and a 50 kpc apocentre (left panel) compared to the same model on a box orbit which has one close pericentre passage at 2 kpc and then continues on a circular orbit at 50 kpc (right panel). For the elliptic orbit, the dE,N is strongly stripped by the first two pericentre passages at 90 and 270 Myr and the final UCD has a size and mass resembling the initial nucleus of the model. For the box orbit, most of the envelope becomes unbound due to the pericentre passage at 90 Myr and subsequently escapes during the orbit at apocentre, while the nucleus remains unaffected by the encounter. The final mass of the object is approximately twice that of the initial nucleus. Since our set-up procedure does not distinguish between nucleus and envelope particles we are unable to determine which particles escape, however, naively one would expect the envelope particles to become unbound before the nucleus particles. Under this assumption all particles in the nucleus would be retained while 50 per cent of the final UCD mass comes from the envelope.

In the right panel of Fig. 5 the final profile has a stellar halo, which is visible as a deviation from a single component profile at a surface brightness of ~ 23 mag arcsec $^{-2}$. In general, for models with a nucleus $r_h = 4$ pc (model 1) stellar haloes become visible for UCDs with sizes larger than $r_h \sim 30$ pc, while for models with a nucleus $r_h = 10$ pc (model 2 and 3) stellar haloes become visible for UCDs with sizes larger than $r_h \sim 50$ -60 pc. For all simulations

the halo does not become apparent until a surface brightness of 22-23 mag arcsec $^{-2}$. For simulation 22 (right panel in Fig. 5), it is unclear whether a halo would be observable because if random Gaussian noise with a standard deviation of 0.2 mag arcsec $^{-2}$ is added to simulate observational uncertainties, the profile is fit well by both a King profile and a two-component profile (King profile with a Sérsic profile for the halo). This indicates that some UCDs which only have a single component surface brightness profile could be composed of the nucleus and remaining envelope from the initial dE,N. However, for the more massive and extended simulated UCDs the stellar halo is clearly visible.

The result that UCDs formed by tidal stripping are composed of stars from both the nucleus and envelope of the progenitor dE,N has an important implication. Nuclei of dE,Ns often have different metallicities from the envelope (Paudel et al. 2011), which suggests that UCDs with two-components, as well as some that have only a single component profile (e.g. right panel in Fig. 5), most likely contain populations with different metallicities or a metallicity gradient. This prediction may be tested with future observations.

Tidal streams are an inevitable consequence of the tidal stripping scenario and therefore must be present if UCDs form in this way. In the right panel of Fig. 5 the final profile is embedded in a tidal stream, which becomes dominant in the surface brightness profile at a surface brightness of ~ 27 mag arcsec $^{-2}$ and a radius of ~ 400 pc. For all simulations the tidal streams have surface brightnesses fainter than ~ 27 mag arcsec $^{-2}$ after 2 Gyr. Only box orbit simulations with 50 kpc apocentres have tidal streams with surface brightnesses brighter than 28 mag arcsec $^{-2}$ in the final profiles, while all other simulations have tidal streams with surface brightnesses fainter than 28 mag arcsec $^{-2}$. It is probable the tidal streams would disperse faster in reality due to sub-structure in the galaxy cluster and thus tidal streams are only likely to be observed around UCDs still undergoing significant stripping.

For both the elliptic and box orbit in Fig. 5 the inner region (within ~ 5 -10 pc) changes little throughout the simulation. By fitting a King profile to the innermost region of the final surface brightness profiles for all models we find the core radius typically changes by less than 10 per cent of the initial core radius of the nucleus (dE,N model 1 has a nucleus core radius of 1.5 pc while dE,N models 2 and 3 both have a nucleus core radius of 3.7 pc). This suggests the surface brightness profiles of UCDs formed by tidal stripping should have the same core radius as their progenitor dE nucleus.

4 DISCUSSION

We have performed simulations of nucleated dwarf galaxies undergoing tidal stripping in a Virgo-like galaxy cluster to form UCDs. Using the particle-mesh code SUPERBOX, we have performed 45 simulations with varying orbital parameters to test the effect of the dwarf galaxy's orbit on the size of the UCD formed due to the stripping of the dwarf's outer envelope.

We find that repeated close passages which occur during elliptic orbits lead to the formation of compact star

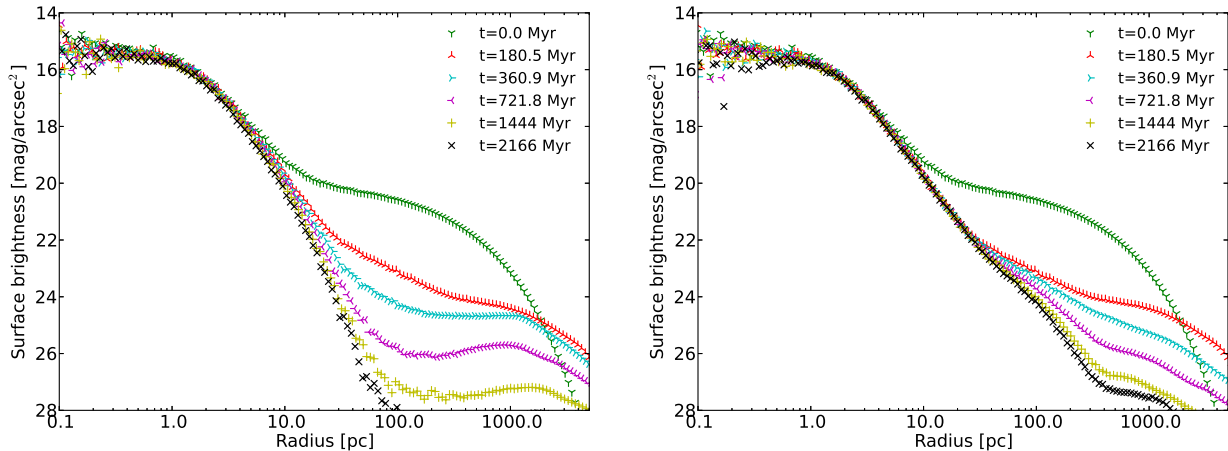


Figure 5. Surface brightness profile evolution over time for dE,N model 1. *Left.* An elliptic with a 2 kpc pericentre and 50 kpc apocentre (Simulation 1 in Table 1, final $r_h = 3.9$ pc, $M_V = -9.77$). *Right.* A box orbit with one pericentre passage at 2 kpc and a 50 kpc apocentre/circular orbit (Simulation 22 in Table 1, final $r_h = 28.3$ pc, $M_V = -10.84$). The surface brightness profile symbols and colours are as in the legend, showing the time since the start of simulation.

clusters/UCDs, and elliptic orbits can only reproduce the full range of UCD sizes if the dE nuclei have half-light radii $r_h > 10$ pc. Given a large fraction of dE nuclei have half-light radii $r_h \sim 4$ pc (including almost all nuclei with luminosities $M_V > -11$), we consider tidal stripping on elliptic orbits unlikely to be the dominant mechanism for UCD formation. In contrast orbital motion in box orbits, or other orbits where very close pericentre passages happen only once or twice and at all other times the stripped dwarf galaxy is far from the centre of a major galaxy, lead to the formation of extended objects resembling UCDs regardless of the nucleus half-light radius. For such box orbits the dwarf galaxies need close pericentre passages with distances less than 10 kpc to undergo strong enough stripping so that UCD formation is possible.

Observations suggest that the nuclei must expand by a factor of two to account for the size difference between UCDs and dE nuclei (Evstigneeva et al. 2008), however we find the nuclei expand little during the tidal stripping process. Instead, the stripped dE,N galaxies can resemble the extended UCDs by retaining more mass than contained within the initial nucleus, causing the UCDs to be more extended. During the stripping process the envelope profile steepens, and in some cases the UCD can appear to have a single component profile despite being composed of both the nucleus and remnant envelope. For all orbits considered in our simulations, the typical UCD size is 2-3 times the initial dE nucleus size, in agreement with the findings of Evstigneeva et al. (2008).

Despite the simulated UCDs having more mass than the initial nucleus, we find only the extended UCDs have stellar haloes. For the dE,N models with a compact nucleus ($r_h = 4$ pc) we find haloes only become visible for objects with a half-light radius greater than ~ 30 pc, while for dE,N models with a larger nucleus ($r_h = 10$ pc) a halo becomes visible for a half-light radius larger than ~ 50 -60 pc. For both nuclei sizes the halo tends to become visible in the surface brightness profile at ~ 22 -23 mag arcsec $^{-2}$ and between ~ 10 -100 pc, however, the position this occurs at for a given UCD will depend strongly on the mass profile of the

progenitor dE,N (in particular on the King concentration for the nucleus and Sersic index for the envelope) and remaining mass in the envelope. Some observed UCDs, in particular the most extended ones, are better fit by two-component models (Evstigneeva et al. 2008), while deviations from single-component King models at a surface brightness of ~ 22 -23 mag arcsec $^{-2}$ can be seen qualitatively in some of the observed surface brightness profiles of UCDs (e.g. the profiles for UCD16 and UCD33), in agreement with our results.

Given our results suggesting the nuclei undergo little expansion and retain the core radius of their progenitor dE nucleus, we predict that high mass UCDs ($M_V < -11$) should have cores ranging up to ~ 20 pc due to the large range in nuclei sizes at higher luminosities, assuming most progenitor nuclei have half-light radii below 20 pc. In contrast, most low mass UCDs should have profiles with cores up to a few parsec, since most nuclei in this range have half-light radii of ~ 4 pc. This range is consistent for the UCDs in the Fornax and Virgo clusters which have King core radii in the range 2-7 pc (Evstigneeva et al. 2008). No surface brightness profiles are available for the extended, low luminosity UCDs ($r_h \sim 40$ pc, $M_V \sim -9$) as yet but this prediction may be tested with future observations.

Although we simulated a dE with a nucleus of $M_V = -12$ and $r_h = 10$ pc (model 3) there also exist many compact nuclei with $M_V = -12$ and $r_h = 4$ pc, as shown in Fig. 2. If the envelope for both dE,Ns is similar, our results from Fig. 4 imply a dE,N with a nucleus of $M_V = -12$ and $r_h = 4$ pc will evolve during tidal stripping in a similar way to model 3, up until $r_h \sim 100$ pc when the nucleus starts to become dominant in the mass profile. After this point the UCD would be more compact than model 3 for a given luminosity, similar to the situation between models 1 and 2. The most massive nuclei in Fig. 2 have $M_V < -14$ and $r_h \sim 40$ pc, however no UCDs are observed at these sizes. Our simulations show that tidally stripped dE,Ns resulting in UCDs less massive and less extended than the initial nucleus requires many (more than 5) pericentre passages with distances less than 5 kpc. We consider such orbits with many

close pericentre passages unlikely since a small perturbation could increase the pericentre distance. As the typical UCD size is 2-3 times the initial nucleus size, UCDs formed from such massive nuclei would likely have sizes of $r_h \sim 100$ pc and luminosities of $M_V \sim -15$. Since the host galaxies of the most massive nuclei are lenticular (S0) or elliptical galaxies, and therefore more massive than dEs, the number of close pericentre passages required to tidally strip the galaxy is likely much larger. The extreme orbits required for formation, and the rarity of objects with such massive nuclei, may explain the lack of objects in this region. An extremely massive nucleus with $M_V = -16$ would most likely resemble a compact elliptical galaxy, rather than a UCD, after tidal stripping.

Two questions that remain unanswered are whether orbits with only one to two close passages required for extended UCD formation occur in real galaxy clusters, and whether dwarf galaxies are destroyed in sufficient numbers to explain all UCDs. For the first question a possible scenario in which such orbits may occur is if the first few passages of a dwarf galaxy in a galaxy cluster are highly radial, due to infall on low-angular momentum orbits, after which the pericentre increases due to a triaxial potential or interactions with other galaxies. A detailed answer to the first question, however, requires following the orbits of dwarf galaxies in cosmological simulations and we defer this, along with more accurate predictions of UCD numbers and spatial distributions, to a future paper.

For the second question, there already exists some previous work constraining the number of possible progenitor galaxies for UCDs. Mieske et al. (2012) compared the specific frequencies of GCs and UCDs around various clusters and found no more than 50 per cent of UCDs may be formed by tidal stripping (based on the error bars of the specific frequencies derived for GCs). In the central ~ 50 -70 kpc of the galaxy clusters they find $\gtrsim 90$ per cent of possible progenitor dwarfs need to be disrupted to account for half of the UCDs. As tidal stripping will be most efficient near the centre of a galaxy cluster we consider it entirely possible that such a high fraction of dwarfs in this region have been tidally disrupted.

To date there have been 34 UCDs discovered in M87, with possibly more than 50 still undiscovered out to a distance of 200 kpc (Brodie et al. 2011). Following Mieske et al. (2012), we assume 50 per cent of the UCDs, ~ 40 , to be formed by tidal stripping. According to the catalogue of Binggeli, Sandage & Tammann (1985), about 50 dEs are located within a projected distance of 200 kpc from the centre of M87 (Peng et al. 2008). Given approximately 70 per cent of dEs are nucleated (Côté et al. 2006; Turner et al. 2012), this leaves 35 dE_Ns to be possible UCD progenitors. Therefore, approximately $\frac{40}{40+35} \approx 53$ per cent of possible UCD progenitor galaxies within 200 kpc of M87 need to be tidally stripped to account for half of the UCDs. It is possible that observations are consistent with a population in which all dwarf galaxies are nucleated (Thomas, Drinkwater & Evstigneeva 2008), which would lower the fraction needed to be stripped by 10 per cent. This estimate is consistent with calculations from cosmological simulations which suggest half of satellite galaxies get disrupted and/or accreted to their host halos (Henriques, Bertone & Thomas 2008).

Alternatively, one could obtain an estimate of accreted dwarf galaxy numbers by looking at the globular cluster systems of elliptical galaxies. Giant elliptical galaxies contain very rich GC systems which are almost universally bimodal in the colour distributions due to differences in metallicity (Brodie & Strader 2006). Dwarf elliptical galaxies on the other hand contain GC systems which are predominantly metal-poor (Peng et al. 2008). One explanation for this bimodality of giant elliptical GCs is that the metal-rich GCs are the intrinsic GC population of the galaxy, or were formed in starbursts triggered by gas-rich mergers, while the metal-poor GCs are provided by accretion of dwarf galaxies (e.g. see the review by Richtler 2012). This explanation is strengthened by current theories of giant elliptical formation where the dominant growth mechanism for the galaxies from $z = 1$ to $z = 0$ is accretion through minor mergers (Naab, Johansson & Ostriker 2009). Two previous studies have investigated the build-up of the GC systems of giant ellipticals via accretion of galaxies: Côté, Marzke & West (1998) for NGC 4472, and Hilker, Infante & Richtler (1999b) for NGC 1399, although using slightly different methods. These techniques provide a useful way to study the accretion of dwarf galaxies by giant ellipticals, however such an analysis is beyond the scope of this paper.

A common origin of accretion and tidal stripping of dwarf galaxies for UCDs and blue GCs in giant ellipticals also places a constraint on the spatial distribution of UCDs. If this scenario is correct, due to their common origin, we expect UCDs far from the centre of M87 to have a similar spatial distribution as the blue GCs. However at small distances UCDs should be underrepresented compared to GCs due to the ongoing tidal stripping converting UCDs into GC-like objects. Some evidence for a more extended distribution of UCDs compared to GCs in the inner regions of galaxy clusters has been found (Hilker 2011; Mieske et al. 2012), in agreement with our expectations.

In summary, we have demonstrated that the extended, low mass UCDs found by Brodie et al. (2011) can be formed in the tidal stripping scenario providing the dwarf galaxies have one or two pericentre passages with distances less than 10 kpc. Given the observed range of dE nuclei sizes and luminosities, the full range of UCD sizes can be produced within the tidal stripping scenario.

ACKNOWLEDGEMENTS

We wish to thank Manuel Metz for providing a GPU enabled version of SUPERBOX, and Michael Drinkwater and the anonymous referee for helpful comments which improved the paper. JP is supported by the University of Queensland via an Australian Postgraduate Award and UQ Advantage RHD Scholarship. HB is supported by the Australian Research Council through Future Fellowship grant FT0991052 and Discovery Project grant DP110102608. Part of this work was performed on the gSTAR national facility at Swinburne University of Technology. gSTAR is funded by Swinburne and the Australian Governments Education Investment Fund.

REFERENCES

- Bassino L. P., Muzzio J. C., Rabolli M., 1994, *ApJ*, 431, 634
- Bekki K., Couch W. J., Drinkwater M. J., 2001, *ApJ*, 552, L105
- Bekki K., and Couch W. J., Drinkwater M. J., Shioya Y., 2003, *MNRAS*, 344, 399
- Binggeli B., Sandage A., Tammann G. A., 1985, *AJ*, 90, 1681
- Binney J., Tremaine S., 1987, *Galactic Dynamics*. Princeton Univ. Press, Princeton
- Brodie J. P., Strader J., 2006, *ARA&A*, 44, 193
- Brodie J. P., Romanowsky A. J., Strader J., Forbes D. A., 2011, *AJ*, 142, 199
- Brüns R. C., Kroupa P., Fellhauer M., Metz M., Assmann P., 2011, *A&A*, 529, A138
- Brüns R. C., Kroupa P., 2012, *A&A*, 547, A65
- Chiboucas K. et al., 2011, *ApJ*, 737, 86
- Chilingarian I. V., 2009, *MNRAS*, 394, 1229
- Chilingarian I. V., Mamon G. A., 2008, *MNRAS*, 385, L83
- Chilingarian I. V., Mieske S., Hilker M., Infante L., 2011, *MNRAS*, 412, 1627
- Côté P., Marzke R. O., West M. J., 1998, *ApJ*, 501, 554
- Côté P. et al., 2006, *ApJS*, 165, 57
- Da Rocha C., Mieske S., Georgiev I. Y., Hilker M., Ziegler B. L., Mendes de Oliveira C., 2011, *A&A*, 525, A86
- Drinkwater M. J., Jones J. B., Gregg M. D., Phillipps S., 2000, *PASA*, 17, 227
- Drinkwater M. J., Gregg M. D., Hilker M., Bekki K., Couch W. J., Ferguson H. C., Jones J. B., Phillipps S., 2003, *Nature*, 423, 519
- Evstigneeva E. A., Gregg M. D., Drinkwater M. J., Hilker M., 2007a, *AJ*, 133, 1722
- Evstigneeva E. A., Drinkwater M. J., Jurek R., Firth P., Jones J. B., Gregg M. D., Phillipps S., 2007b, *MNRAS*, 378, 1036
- Evstigneeva E. A. et al., 2008, *AJ*, 136, 461
- Fellhauer M., Kroupa P., Baumgardt H., Bien R., Boily C. M., Spurzem R., Wassmer N., 2000, *New A*, 5, 305
- Fellhauer M., Kroupa P., 2002, *MNRAS*, 330, 642
- Francis K. J., Drinkwater M. J., Chilingarian I. V., Bolt A. M., Firth P., 2012, *MNRAS*, 425, 325
- Geha M., Guhathakurta P., van der Marel R. P., 2002, *AJ*, 124, 3073
- Geha M., Guhathakurta P., van der Marel R. P., 2003, *AJ*, 126, 1794
- Ghigna S., Moore B., Governato F., Lake G., Quinn T., Stadel J., 1998, *MNRAS*, 300, 146
- Goerdt T., Moore B., Kazantzidis S., Kaufmann T., Macciò A. V., Stadel J., 2008, *MNRAS*, 385, 2136
- Grant N. I., Kuipers J. A., Phillipps S., 2005, *MNRAS*, 363, 1019
- Hau G. K. T., Spitler L. R., Forbes D. A., Proctor R. N., Strader J., Mendel J. T., Brodie J. P., Harris W. E., 2009, *MNRAS*, 394, L97
- Hasegan M. et al., 2005, *ApJ*, 627, 203
- Henriques B. M., Bertone S., Thomas P. A., 2008, *MNRAS*, 383, 1649
- Hilker M., Infante L., Vieira G., Kissler-Patig M., Richtler T., 1999a, *A&AS*, 134, 75
- Hilker M., Infante L., Richtler T., 1999b, *A&AS*, 138, 55
- Hilker M., Baumgardt H., Infante L., Drinkwater M., Evstigneeva E., Gregg M., 2007, *A&A*, 463, 119
- Hilker M., 2011, *EAS Publ. Ser.*, 48, 219
- Jones J. B. et al., 2006, *AJ*, 131, 312
- King I., 1962, *AJ*, 67, 471
- Kormendy J., Fisher D. B., Cornell M. E., Bender R., 2009, *ApJS*, 182, 216
- Kroupa P., 1998, *MNRAS*, 300, 200
- Madrid J. P., *ApJ*, 2011, 737, L13
- Mieske S., Hilker M., Infante L., 2002, *A&A*, 383, 823
- Mieske S. et al., 2004, *AJ*, 128, 1529
- Mieske S., Hilker M., Infante L., Jordán A., 2006, *AJ*, 131, 2442
- Mieske S., Hilker M., Jordán A., Infante L., Kissler-Patig M., 2007, *A&A*, 472, 111
- Mieske S. et al., 2008, *A&A*, 487, 921
- Mieske S., Hilker M., Misgeld I., 2012, *A&A*, 537, A3
- Miller B. W., Lotz J. M., 2007, *ApJ*, 670, 1074
- Misgeld I., Mieske S., Hilker M., Richtler T., Georgiev I. Y., Schuberth Y., *A&A*, 2011, 531, A4
- Murphy J. D., Gebhardt K., Adams J. J., 2011, *ApJ*, 729, 129
- Naab T., Johansson P. H., Ostriker J. P., 2009, *ApJ*, 699, L178
- Norris M. A., Kannappan S. J., 2011, *MNRAS*, 414, 739
- Paudel S., Lisker T., Kuntschner H., 2011, *MNRAS*, 413, 1764
- Peñarrubia J., Benson A. J., Walker M. G., Gilmore G., McConnachie A. W., Mayer L., 2010, *MNRAS*, 406, 1290
- Peng E. W. et al., 2006, *ApJ*, 639, 838
- Peng E. W. et al., 2008, *ApJ*, 681, 197
- Penny S. J., Forbes D. A., Conselice C. J., *MNRAS*, 2012, 422, 885
- Prugniel P., Simien F., *A&A*, 321, 111
- Richtler T., Dirsch B., Larsen S., Hilker M., Infante L., 2005, *A&A*, 439, 533
- Richtler T., 2012, preprint (astro-ph/1210.0045)
- Sérsic J. L., 1963, *Boletín de la Asociación Argentina de Astronomía*, 6, 41
- Sérsic J. L., 1968, *Atlas de Galaxias Australes*. Observatorio Astronómico, Córdoba
- Terzić B., Graham A. W., 2005, *MNRAS*, 362, 197
- Thomas P. A., Drinkwater M. J., Evstigneeva E., 2008, *MNRAS*, 389, 102
- Trager S. C., King I. R., Djorgovski S., 1995, *AJ*, 109, 218
- Turner M. L., Cote P., Ferrarese L., Jordan A., Blakeslee J. P., Mei S., Peng E. W., West M. J., 2012, *ApJS*, 203, 5